



**HAL**  
open science

## A finite-volume tracking scheme for two-phase compressible flow

Christophe Chalons, Jim Magiera, Christian Rohde, Maria Wiebe

► **To cite this version:**

Christophe Chalons, Jim Magiera, Christian Rohde, Maria Wiebe. A finite-volume tracking scheme for two-phase compressible flow. 16th International Conference on Hyperbolic Problems: Theory, Numerics and Applications, 2016, Aug 2016, Aachen, Germany. pp.309-322, 10.1007/978-3-319-91545-6\_25 . hal-03993095

**HAL Id: hal-03993095**

**<https://hal.science/hal-03993095>**

Submitted on 28 Feb 2023

**HAL** is a multi-disciplinary open access archive for the deposit and dissemination of scientific research documents, whether they are published or not. The documents may come from teaching and research institutions in France or abroad, or from public or private research centers.

L'archive ouverte pluridisciplinaire **HAL**, est destinée au dépôt et à la diffusion de documents scientifiques de niveau recherche, publiés ou non, émanant des établissements d'enseignement et de recherche français ou étrangers, des laboratoires publics ou privés.

Copyright

# A Finite-Volume Tracking Scheme for Two-Phase Compressible Flow

Christophe Chalons, Jim Magiera, Christian Rohde and Maria Wiebe

**Abstract** We propose a Finite-Volume tracking method in multiple space dimensions to approximate weak solutions of the hydromechanical equations that allow two-phase behaviour. The method relies on a moving mesh ansatz such that the phase boundary is represented as a sharp interface without any artificial smearing. At the interface an approximate solver is applied, such that the exact Riemann solution is not required. From precedent work it is known that the method is locally conservative and recovers planar traveling wave solutions exactly. To demonstrate the efficiency and reliability of the new scheme we test it on various situations for liquid-vapour flow.

**Key words:** Sharp interface resolution, compressible two-phase flow, moving mesh method, Finite-Volume scheme, phase transition

*Subject Classifications:* 35L65, 76M25, 76T10, 65M50

## 1 Introduction

We consider weak solutions of the Euler equations for compressible two-phase flow. This system is equipped with an entropy-entropy flux pair such that the entropy is strictly convex in a state space that is split into two disjoint open subsets - the liquid and the vapour bulk. The separating set is called spinodal region. As a consequence one has strict hyperbolicity in the complete state space. Phase boundaries are considered as shock waves that connect states in different phases in a subsonic way. In

---

Christophe Chalons  
Laboratoire de Mathématiques de Versailles, UVSQ, CNRS, Université Paris-Saclay, 78035 Versailles, France e-mail: christophe.chalons@uvsq.fr

Christian Rohde/Jim Magiera/Maria Wiebe  
Institute for Applied Analysis and Numerical Simulation, University of Stuttgart, Pfaffenwaldring 57, D-70569 Stuttgart, Germany, e-mail: crohde/jim.magiera/maria.wiebe@mathematik.uni-stuttgart.de

this way the spinodal region can be avoided. Phase boundaries still have to satisfy the entropy inequality, thus being consistent with the second law of thermodynamics. Nevertheless well-posedness in the setting of two disjoint state spaces must be restored with additional constraints, e.g. so-called kinetic relations [17], which are put on the phase boundary.

The numerical approximation of problems with phase boundaries is a challenging issue: To avoid approximate solutions with values outside of the state space advanced techniques like the precise tracking of the interface are required. In this contribution we use the approach [5], extended to the two-phase Euler system. It relies on the tracking of the phase boundary using a moving mesh and exploiting the exact dynamics across phase boundaries. The moving mesh approach in this paper is different from standard uses where the mesh is changed globally to reduce the error or to get aligned with appropriate transport directions. Here we intend to track the mesh only locally around the discrete interface and try to avoid any global changes of the mesh that effect the bulk domains.

In the paper at hand we present a specific approach for the two-phase Euler equations. In particular we present pertinent numerical tests in one and two space dimensions. For the general approach and for analytical results we refer to [6]. Another approach for the numerical treatment of phase boundaries in compressible liquid-vapour flow is e.g. the ghostfluid method [10, 11]. Mixed phase volumes for compressible multi-phase flow are allowed in [8] where also the moving-mesh approach is used.

## 2 Isothermal Euler equations

The isothermal Euler equations with non-monotone pressure function govern the dynamics of compressible liquid-vapour flow. Assume that a time  $T \in (0, \infty)$  and a time-space domain  $D_T = \mathbb{R}^d \times (0, T)$  are given. Then the isothermal Euler equations read as

$$\begin{pmatrix} \rho \\ \rho \mathbf{v} \end{pmatrix}_t + \nabla \cdot \begin{pmatrix} \rho \mathbf{v} \\ \rho \mathbf{v} \otimes \mathbf{v} + p(\rho) \mathbf{I} \end{pmatrix} = 0 \text{ in } D_T. \quad (1)$$

The unknowns are the density  $\rho = \rho(t, \mathbf{x})$  and the momentum  $\rho \mathbf{v}$  where  $\mathbf{v} = (v_1(t, \mathbf{x}), \dots, v_d(t, \mathbf{x}))^T$  denotes the velocity of the fluid. With  $\mathbf{u} = (\rho, \rho \mathbf{v})$  and a suitable flux function  $\mathbf{f}$  system (1) can be rewritten as

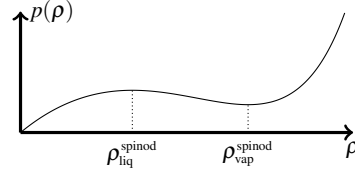
$$\mathbf{u}_t + \nabla \cdot \mathbf{f}(\mathbf{u}) = 0.$$

The given pressure function  $p$  is chosen in Van-der-Waals form

$$p : (0, B^{-1}) \rightarrow \mathbb{R}^+, \rho \mapsto R\theta \frac{\rho}{1 - B\rho} - A\rho^2, \quad (2)$$

with positive constants  $A, B, \theta, R > 0$ , where the fixed temperature  $\theta$  is chosen in the subcritical regime such that  $p$  is non-monotone (see Figure 1). We denote by  $\rho_{\text{liq}}^{\text{spinod}} < \rho_{\text{vap}}^{\text{spinod}}$  the extreme values of the interval where the pressure function  $p$  is

**Fig. 1** Pressure function  $p = p(\rho)$ , which defines the phases of a fluid by the domains where  $p$  is monotone increasing.



decreasing. The density must not take values in the interval  $(\rho_{\text{liq}}^{\text{spinod}}, \rho_{\text{vap}}^{\text{spinod}})$ , i.e.

$$\rho : [0, T] \times \mathbb{R}^d \rightarrow (0, \rho_{\text{liq}}^{\text{spinod}}] \cup [\rho_{\text{vap}}^{\text{spinod}}, B^{-1}).$$

Therefore we define liquid and vapour bulk states according to

$$\mathcal{P}_- = (0, \rho_{\text{liq}}^{\text{spinod}}] \times \mathbb{R}^d, \quad \mathcal{P}_+ = [\rho_{\text{vap}}^{\text{spinod}}, B^{-1}) \times \mathbb{R}^d, \quad (3)$$

and define the state space  $\mathcal{U}$  as the union of both sets  $\mathcal{U} = \mathcal{P}_- \cup \mathcal{P}_+ \subset \mathbb{R}^m$ . We distinguish the phases by a mapping  $\pi$  given as

$$\pi : \mathcal{U} \rightarrow \{-, +\}, \mathbf{u} \mapsto \begin{cases} - & \text{if } \mathbf{u} \in \mathcal{P}_-, \\ + & \text{if } \mathbf{u} \in \mathcal{P}_+. \end{cases} \quad (4)$$

In the following we will consider an initial state  $\mathbf{u}_0 = (\rho_0, \rho_0 \mathbf{v}_0)$ , such that

$$(\rho, \rho \mathbf{v})(0, \cdot) = (\rho_0, \rho_0 \mathbf{v}_0). \quad (5)$$

A function  $\mathbf{u} \in L^\infty((0, T) \times \mathbb{R}^d, \mathcal{U})$  is called a **weak solution** of the initial value problem (1), (5) in  $D_T$  if

$$\int_0^T \int_{\mathbb{R}^d} \mathbf{u} \phi_t + \mathbf{f}(\mathbf{u}) \cdot \nabla \phi \, dV \, dt = - \int_{\mathbb{R}^d} \mathbf{u}_0 \phi(0, \mathbf{x}) \, dV$$

holds for all  $\phi \in \mathcal{C}_0^\infty([0, T] \times \mathbb{R}^d, \mathbb{R})$ .

The system (1) is equipped with an entropy-entropy flux pair  $(\eta, \mathbf{q}) : \mathcal{U} \rightarrow \mathbb{R}^{d+1}$ . The canonical entropy-entropy flux pair for (1) is given by

$$\eta(\rho, \mathbf{m}) = \rho \Psi(\rho) + \frac{|\mathbf{m}|^2}{2\rho}, \quad \mathbf{q}(\rho, \mathbf{m}) = (q_1(\rho, \mathbf{m}), \dots, q_d(\rho, \mathbf{m})) = \frac{\mathbf{m}}{\rho} (\eta + p(\rho)),$$

with  $\Psi$  such that  $\Psi'(\rho) = \frac{p(\rho)}{\rho^2}$ . A weak solution  $\mathbf{u} \in L^\infty((0, T) \times \mathbb{R}^d, \mathcal{U})$  is called an **entropy solution** of (1), (5) in  $D_T$  if

$$\int_0^T \int_{\mathbb{R}^d} \eta(\mathbf{u}) \phi_t + \mathbf{q}(\mathbf{u}) \cdot \nabla \phi \, dV \, dt \geq - \int_{\mathbb{R}^d} \eta(\mathbf{u}_0) \phi(0, \mathbf{x}) \, dV \quad (6)$$

holds for all  $\phi \in \mathcal{C}_0^\infty([0, T] \times \mathbb{R}^d, \mathbb{R})$ ,  $\phi \geq 0$ .

It is well known (cf. [2]) that single phase boundaries do not only have to satisfy

the Rankine-Hugoniot conditions but also an additional so-called kinetic relation. Following [12] we require for some function  $\mathcal{K} : \mathcal{P}_- \times \mathcal{P}_+ \times \mathbb{R} \rightarrow \mathbb{R}$  that all phase boundaries connecting  $\mathbf{u}_-$  with  $\mathbf{u}_+$  with velocity  $r$  satisfy the kinetic relation

$$\mathcal{K}(\mathbf{u}_-, \mathbf{u}_+, r) = 0 \quad (7)$$

where

$$\mathcal{K}(\mathbf{u}_-, \mathbf{u}_+, r) = \mu(\rho_-) + 0.5(\mathbf{v}_- \cdot \mathbf{n} - r)^2 - \mu(\rho_+) - 0.5(\mathbf{v}_+ \cdot \mathbf{n} - r)^2 + k_* j,$$

with the Gibb's free energy  $\mu$  given through  $\mu' = p'/\rho$ , relative mass flux  $j = \rho_- (\mathbf{v}_- \cdot \mathbf{n} - r)$  and mobility  $k_* > 0$ . In this paper we are interested in entropy solutions  $\mathbf{u}$  that split  $\mathbb{R}^d$  for each time  $t \in [0, T)$  in two disjunct  $\pm$ -phase domains  $D_-(t), D_+(t)$  and a hypersurface  $\Gamma(t)$  such that for almost all  $\mathbf{x} \in \mathbb{R}^d$

$$\pi \mathbf{u}(t, \mathbf{x}) = \pm \Rightarrow \mathbf{x} \in D_{\pm}(t) \quad (8)$$

and  $\Gamma(t) = \overline{D_-(t)} \cap \overline{D_+(t)}$  hold. We call  $D_{\pm}(t)$  the  $\pm$ -*phase domain* and  $\Gamma(t)$  the *sharp interface*. For  $\mathbf{x} \in \Gamma(t)$  let  $\mathbf{n}(t, \mathbf{x}) = (n_1(t, \mathbf{x}), \dots, n_d(t, \mathbf{x}))^T \in \mathcal{S}^1$  denote the normal vector of  $\Gamma(t)$  that points into  $D_-(t)$ . Let the function  $\mathbf{u} : D_T \rightarrow \mathcal{U}$  be regular enough such that for  $(t, \mathbf{x}) \in D_T$  the traces

$$\mathbf{u}_{\pm}(t, \mathbf{x}) := \lim_{\varepsilon \rightarrow 0, \varepsilon > 0} \mathbf{u}(t, \mathbf{x} \pm \varepsilon \mathbf{n}(t, \mathbf{x}))$$

exist. Then we define the interfacial jump for  $\mathbf{x} \in \Gamma(t)$  by

$$\llbracket \mathbf{u}(t, \mathbf{x}) \rrbracket = \mathbf{u}_+(t, \mathbf{x}) - \mathbf{u}_-(t, \mathbf{x}).$$

We denote by  $r(t, \mathbf{x})$  the speed of  $\Gamma(t)$  in direction  $\mathbf{n}(t, \mathbf{x})$ . Necessary conditions for the function  $\mathbf{u}$  to be a weak solution of (1), (5) are the Rankine-Hugoniot conditions

$$-r(t, \cdot) \llbracket \mathbf{u}(t, \cdot) \rrbracket + \llbracket \mathbf{n} \cdot \mathbf{f}(\mathbf{u}(t, \cdot)) \rrbracket = 0. \quad (9)$$

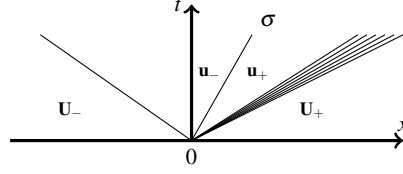
In the given setting a function  $\mathbf{u} \in C^0([0, T); L^\infty(\mathbb{R}^d))$ ,  $\pm$ -phase domain families  $\{D_{\pm}(t)\}_{t \in [0, T)}$  and a sharp-interface family  $\{\Gamma(t)\}_{t \in [0, T)}$  are called an *entropy-compatible sharp-interface solution of (1), (5)* if the following conditions hold.

- (i) For  $t = 0$  we have  $D_{\pm}(0) = D_{\pm,0}$ ,  $\Gamma(0) = \Gamma_0$ , and for each  $t \in (0, T)$  we have  $\mathbb{R}^d = D_-(t) \cup D_+(t) \cup \Gamma(t)$  with disjunct  $d$ -dimensional  $\pm$ -phase domains  $D_{\pm}(t)$  and the hypersurface  $\Gamma(t)$ .
- (ii) The condition (8) holds for almost all  $(t, \mathbf{x}) \in D_T$ .
- (iii) The function  $\mathbf{u}$  is an entropy solution of (1), (5) in  $D_T$ .
- (iv) For each  $t \in (0, T)$  the function  $\mathbf{u}$  satisfies the trace conditions (7), (9).

For our numerical approach the Riemann problem for the planar situation of (1) will be important. Fix some  $\mathbf{n} \in \mathcal{S}^{d-1}$  and define

$$\mathbf{F}(\mathbf{u}) = n_1 \mathbf{f}_1(\mathbf{u}) + \dots + n_d \mathbf{f}_d(\mathbf{u}), \quad \mathbf{u} \in \mathcal{U}. \quad (10)$$

**Fig. 2** Sketch of a Riemann pattern that contains a phase transition wave with speed  $\sigma$ . The adjacent states are  $\mathbf{u}_\pm \in \mathcal{P}_\pm$ .



Then for states  $\mathbf{U}_\pm \in \mathcal{P}_\pm$ , the Riemann problem is the special initial value problem

$$\mathbf{w}_t + (\mathbf{F}(\mathbf{w}))_x = 0 \text{ in } (0, \infty) \times \mathbb{R}, \quad \mathbf{w}(0, x) = \begin{cases} \mathbf{U}_- & \text{if } x < 0, \\ \mathbf{U}_+ & \text{if } x > 0, \end{cases} \quad (11)$$

with unknown  $\mathbf{w} = \mathbf{w}(t, x) \in \mathcal{U}$ . It is a reasonable assumption that the exact entropy solution  $\mathbf{w}$  of (11) is a self-similar function that connects the left state  $\mathbf{U}_-$  and the right state  $\mathbf{U}_+$  by at most 3 (for  $m$ -dimensional systems at most  $m$ ) elementary waves (i.e., shock waves, contact waves, rarefaction waves, attached shock-rarefaction waves, each of them within either  $\mathcal{P}_-$  or  $\mathcal{P}_+$ ) and exactly one phase transition wave. The phase boundary wave is a shock wave that connects a state  $\mathbf{u}_-$  in  $\mathcal{P}_-$  with a state  $\mathbf{u}_+$  in  $\mathcal{P}_+$ . Across this wave the conditions (9), (7) have to hold (see [13] for a general theory and [7, 9, 12, 14, 15] for specific cases). The range of the function  $\mathbf{w}$  is in  $\mathcal{P}_-$  left to the phase transition and in  $\mathcal{P}_+$  otherwise (see Figure 2 for some illustration). In the following, we do not need to know the exact Riemann problem solution but only the speed of the phase transition, as well as the two adjacent values. This might be even given by an approximate solver [4, 16]. To combine both cases we introduce an interface solver. For some kinetic relation (7) the mapping  $\mathcal{R}_\mathbf{F}: \mathcal{P}_- \times \mathcal{P}_+ \rightarrow \mathbb{R} \times \mathcal{P}_- \times \mathcal{P}_+$  with

$$\mathcal{R}_\mathbf{F}(\mathbf{U}_-, \mathbf{U}_+) := (\sigma, \mathbf{u}_-, \mathbf{u}_+) \quad (12)$$

is called an *interface solver* for (1) if the following conditions are satisfied.

- (i)  $\mathcal{R}_\mathbf{F}$  is a continuous mapping.
- (ii) The states  $\mathbf{u}_\pm \in \mathcal{P}_\pm$  and  $\sigma$  satisfy

$$-\sigma(\mathbf{u}_- - \mathbf{u}_+) + \mathbf{F}(\mathbf{u}_-) - \mathbf{F}(\mathbf{u}_+) = 0, \quad \mathcal{H}(\mathbf{u}_-, \mathbf{u}_+, \sigma) = 0. \quad (13)$$

- (iii) If there is a  $r \in \mathbb{R}$  such that  $\mathbf{U}_-, \mathbf{U}_+$  fulfill (13) with  $\sigma = r$  then  $\mathcal{R}_\mathbf{F}(\mathbf{U}_-, \mathbf{U}_+) = (r, \mathbf{u}_-, \mathbf{u}_+)$ .

We call  $\sigma$  the *speed of the interface*.

### 3 A FV Moving Mesh Method with Interface Tracking

In this section we shortly summarize the used numerical method from [6] for multiple space dimensions. The method is a Finite Volume scheme on moving meshes

combined with an interface tracking and a post-processing step where the mesh is improved with regard to the volume/perimeter ratio.

Assume that a (fixed) mesh is given as set of  $(d+1)$ -polygons  $K_i$  ( $i \in I$  index set), i.e.  $\tau = \{K_i | K_i \in P_{d+1}, i \in I\}$  fulfilling the standard requirements of a mesh in  $\mathbb{R}^d$ . Then we call the pair  $\mathcal{S} = (\tau, \{\Phi_i\}_{i \in I})$  a *moving mesh* with continuous functions

$$\Phi_i : [t_1, t_2] \rightarrow \mathcal{L}_a(K_i, \mathbb{R}^d), t \mapsto \Phi_i^t, \quad \Phi_i(t_1) = \text{id},$$

mapping from an interval to the space of affine mappings  $\mathcal{L}_a(K_i, \mathbb{R}^d)$  from  $K_i$  to  $\mathbb{R}^d$ , if for all  $t \in [t_1, t_2]$  the set  $\{\Phi_i^t(K_i)\}_{i \in I}$  is a (fixed) mesh with index set  $I$ .

This enables us to define the time dependent elements and the time dependent edges as

$$K_i(t) := \Phi_i^t(K_i), \quad S_{i,j}(t) := \Phi_i^t(\overline{K_i} \cap \overline{K_j}).$$

A Finite Volume scheme on a moving mesh then reads

$$|K_i(t^{n+1})| \mathbf{u}_i^{n+1} = |K_i(t^n)| \mathbf{u}_i^n - \Delta t^n \sum_{j \in N(i)} |S_{i,j}(t^{n+1/2})| \left( \mathbf{g}_{i,j}^n(\mathbf{u}_i^n, \mathbf{u}_j^n) + \mathbf{h}_{i,j}^n(\mathbf{u}_i^n, \mathbf{u}_j^n) \right),$$

with  $t^{n+1/2} = t^n + 0.5\Delta t$ . The numerical flux function  $\mathbf{g}_{i,j}^n$  and the geometrical flux function  $\mathbf{h}_{i,j}^n$  are L-continuous functions, which obey the consistency condition

$$\mathbf{g}_{i,j}^n(\mathbf{u}, \mathbf{u}) = \mathbf{f}(\mathbf{u}) \cdot \mathbf{n}_{i,j}(t^{n+1/2})$$

as well as the conservation property

$$\mathbf{g}_{i,j}^n(\mathbf{u}, \mathbf{v}) + \mathbf{h}_{i,j}^n(\mathbf{u}, \mathbf{v}) = - \left( \mathbf{g}_{j,i}^n(\mathbf{v}, \mathbf{u}) + \mathbf{h}_{j,i}^n(\mathbf{v}, \mathbf{u}) \right).$$

The idea of the scheme in [6] is to choose the mappings  $\Phi_i$  (and thus the time dependent elements  $K_i(t)$ ) with the aid of the interface solver  $\mathcal{B}_F$  such that the position of the phase transition is tracked. This has two advantages: First, we can treat interface edges separately via making a special choice for numerical and geometrical fluxes  $\mathbf{g}_{i,j}^n(\mathbf{u}, \mathbf{v})$  and  $\mathbf{h}_{i,j}^n(\mathbf{u}, \mathbf{v})$  when  $\pi(\mathbf{u}) \neq \pi(\mathbf{v})$ . Secondly, we do not have any smearing across the interface hypersurface due to averaging, since the phases are sharply separated.

In an additional post-processing step we define a new mesh in order to maintain a decent volume to perimeter ratio of the mesh triangles that might become either very small or very big due to the interface tracking. In our implementation the mesh is chosen as a Constrained Delaunay Traingulation, which provides methods for insertion and removal of points. The complete description of the remeshing algorithm is out of scope. Let us mention that the remeshing, realized by point insertion and removal leads only to small changes of the mesh, e.g. the insertion causes 6 new triangles in expectation [3]. In the numerical Example 2 of Section 4.2 we verify this by comparing the meshes before and after remeshing.

The two most important properties of the complete scheme are the following.

- The scheme fulfills the conservation property

$$\int_{\mathbb{R}^d} (\mathbf{u}_h(t^n, \cdot) - \mathbf{u}_0) \, dV = 0,$$

which does not hold e.g. for the ghost fluid method for two-phase problems.

- Assume that an entropy-compatible sharp-interface solution of (1), (5) is given as

$$\mathbf{u}(t, \mathbf{x}) = \begin{cases} \mathbf{u}_L \in \mathcal{P}_- & \text{if } \mathbf{x} \cdot \boldsymbol{\nu} + ct < 0 \\ \mathbf{u}_R \in \mathcal{P}_+ & \text{if } \mathbf{x} \cdot \boldsymbol{\nu} + ct > 0, \end{cases} \quad D_{\pm}(t) = \{\mathbf{x} \in \mathbb{R}^d \mid \mathbf{x} \cdot \boldsymbol{\nu} + ct \leq 0\}.$$

Then the algorithm is able to resolve  $\mathbf{u}$  exactly independent of the coarsity of the mesh when the numerical and geometrical fluxes are chosen as

$$\mathbf{g}_{i,j}^n(\mathbf{u}, \mathbf{v}) = \begin{cases} \mathbf{f}(\mathbf{U}(\mathbf{u}, \mathbf{v})) \cdot \mathbf{n}_{i,j} & \text{if } \mathbf{u} \in \mathcal{P}_-, \mathbf{v} \in \mathcal{P}_+, \\ \mathbf{f}(\mathbf{U}(\mathbf{v}, \mathbf{u})) \cdot \mathbf{n}_{i,j} & \text{if } \mathbf{u} \in \mathcal{P}_+, \mathbf{v} \in \mathcal{P}_-, \\ \tilde{\mathbf{g}}_{i,j}^n(\mathbf{u}, \mathbf{v}) & \text{otherwise,} \end{cases}$$

$$\mathbf{h}_{i,j}^n(\mathbf{u}, \mathbf{v}) = \begin{cases} -\sigma(\mathbf{u}, \mathbf{v})\mathbf{U}(\mathbf{u}, \mathbf{v}) & \text{if } \mathbf{u} \in \mathcal{P}_-, \mathbf{v} \in \mathcal{P}_+, \\ +\sigma(\mathbf{v}, \mathbf{u})\mathbf{U}(\mathbf{v}, \mathbf{u}) & \text{if } \mathbf{u} \in \mathcal{P}_+, \mathbf{v} \in \mathcal{P}_-, \\ \tilde{\mathbf{h}}_{i,j}^n(\mathbf{u}, \mathbf{v}) & \text{otherwise,} \end{cases}$$

where the values  $\sigma(\mathbf{u}, \mathbf{v})$ ,  $\mathbf{U}(\mathbf{u}, \mathbf{v})$  and  $\mathbf{V}(\mathbf{u}, \mathbf{v})$  are obtained from the interface solver  $\mathcal{R}_{\mathbf{f}, \mathbf{n}_{i,j}}$  (see (12))

$$(\sigma(\mathbf{u}, \mathbf{v}), \mathbf{U}(\mathbf{u}, \mathbf{v}), \mathbf{V}(\mathbf{u}, \mathbf{v})) = \mathcal{R}_{\mathbf{f}, \mathbf{n}_{i,j}}(\mathbf{u}, \mathbf{v})$$

and  $\tilde{\mathbf{g}}_{i,j}^n, \tilde{\mathbf{h}}_{i,j}^n$  are arbitrary numerical and geometrical fluxes, respectively.

For a detailed explanation and proofs in two-space dimensions we refer to [6].

## 4 Numerical Results

In this section we will present numerical results for the two-dimensional isothermal Euler equations (1) and Van-der-Waals pressure (2) with constants  $A = 3$ ,  $B = \frac{1}{3}$ ,  $\theta = 0.85$  and  $R = \frac{8}{3}$ . This gives us a state space that is separated by an interval, the unstable spinodal region, into two sets, cf. (3). The construction of an interface solver that allows for entropy compatible sharp-interface solutions has just recently been established in full generality (see [18], and [9] for the framework). Since the details of the construction are not important in the sequel we skip them referring to [18]. In the following examples we apply two kinds of interface solvers, namely an exact and an approximate Riemann solver.

### 4.1 Numerical Results for the one-dimensional Euler equations

As a first example we show numerical results, where we apply the scheme from Section 3 reduced to the one-dimensional case. In one space dimension the phase transitions boils down to a single point and the interface tracking consists of tracking the position of a moving cell edge in the computational mesh. The one-dimensional Euler equations are given by

$$\begin{aligned} \rho_t + (\rho v)_x &= 0 \\ (\rho v)_t + (\rho v^2 + p(\rho))_x &= 0, \end{aligned} \quad (14)$$

with fluid density  $\rho(t, x)$ , scalar velocity  $v(t, x)$  (in  $x$ -direction) and given pressure function  $p(\rho)$ . For the interface solver, we take in this example the Relaxation Riemann solver from [16]. The Relaxation Riemann solver is an approximate Riemann solver and does in general not return the exact Riemann solution, but satisfies the properties of an interface solver, see (i),(ii),(iii) on p. 5.

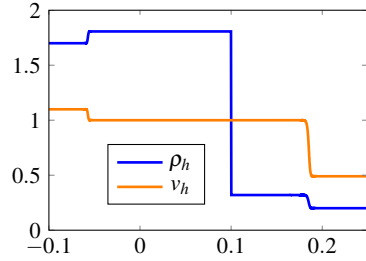


**Fig. 3:** Numerical solution of the 1-d Euler equations for the initial data (15) at time  $t = 0.5$ . We used a mesh with 1000 cells.

$ \tau $	$h(\tau)$	$\ (\mathbf{u}_h - \mathbf{u})(t, \cdot)\ _{L^1}$	EOC
80	$2.50 \cdot 10^{-2}$	0.01895	0.64
160	$1.25 \cdot 10^{-2}$	0.01215	0.72
320	$6.25 \cdot 10^{-3}$	0.00736	0.77
640	$3.13 \cdot 10^{-3}$	0.00430	0.82
1280	$1.56 \cdot 10^{-3}$	0.00243	0.90
2560	$7.81 \cdot 10^{-4}$	0.00130	0.96
5120	$3.91 \cdot 10^{-4}$	0.00067	0.80
10240	$1.95 \cdot 10^{-4}$	0.00039	1.20
20480	$9.77 \cdot 10^{-5}$	0.00017	

**Table 1:**  $L^1$ -errors und EOCs for the numerical scheme for solving the Riemann problem (14), (15). By  $h(\tau)$  we denote the mesh width.

*Example 1.* We check the quality of the scheme by a problem with known exact solution  $\mathbf{u}$ . It consists of four constant states connect via two shock waves and one phase transition

$$\mathbf{u}(t, x) = \begin{cases} (1.7, 1.0992) & : x < s_1 t, \\ (1.8074, 1) & : s_1 t < x < s_2 t, \\ (0.3197, 1) & : s_2 t < x < s_3 t, \\ (0.2, 0.4903) & : s_3 t < x, \end{cases} \quad \mathbf{u}_0 = \mathbf{u}(0, \cdot), \quad (15)$$

with wave speeds  $s_1 = -0.574$ ,  $s_2 = 1$  and  $s_3 = 1.8515$  (all numbers rounded to 4 digits). Figure 3 depicts the numerical approximation. The experimental orders of

convergence (EOC) are presented in Table 1 and show that the EOC tends to 1. This convergence rate might be expected for a single shock wave. Thus one can conclude that the overall approach works, also with an inexact solver.

## 4.2 Numerical Results for the two-dimensional Euler equations

We will conclude this work with numerical examples for the two-dimensional isothermal Euler equations. We perform the computations on the bounded domain  $\Omega := (-1, 1)^2$  in all cases. Appropriate boundary conditions are given for each test case.

The realization of the interface tracking and the remeshing operator was done with the 2D Triangulation package of the C++ library CGAL [1]. Its `Constrained_Delaunay_triangulation_2` class in combination with the hierarchy structure was extended to implement the moving mesh. This class manages a triangulation that is almost Delaunay except for a set of given constraints (in our case: prescribed edges of the interface curve) and it provides methods for the insertion, removal and motion of points.

For the computation of the numerical and geometrical fluxes, we will consider the one-dimensional problem (11). It is easy to see, that the problem with the three unknown  $(\rho, \rho v_1, \rho v_2)$  can be rewritten as the one-dimensional Euler equations (14) with density and the projected momentum  $\rho v_p = \rho \mathbf{v} \cdot \mathbf{n} = \rho(v_1 n_1 + v_2 n_2)$  as unknown. In fact, the used interface solver from [18] applies to this system which readily can be used to design an interface solver.

*Example 2 (Riemann problem).* We start with a validation example and take initial conditions that correspond to a one-dimensional Riemann problem, where the entropy-compatible solution is known. At the boundary we apply absorbing boundary conditions. The entropy solution under investigation consists out of two shock waves with velocities  $s_1 = -1.2960$ ,  $s_3 = 1.5928$  and one phase transition with velocity  $s_2 = 0.2185$  which is given as

$$(\rho(t, \mathbf{x}), \rho \mathbf{v}(t, \mathbf{x})) = \begin{cases} (0.2, 0, 0) & \text{if } x_1 < s_1 t, \\ (0.2646, -0.0837, 0) & \text{if } s_1 t < x_1 < s_2 t, \\ (1.8094, 0.2538, 0) & \text{if } s_2 t < x_1 < s_3 t, \\ (1.65, 0, 0) & \text{if } s_3 t < x_1. \end{cases}$$

Figure 4 shows the numerical solution. One can clearly see that the phase-transition in the middle is resolved as a sharp vertical line while the two neighboring shock waves are slightly smeared out. With the exact solution we compute  $L^1$ -errors and the (experimental) orders of convergence, see Table 2. The errors and the orders listed in Table 2 show that we obtain again convergence with order close to 1. This means that the treatment of the phase transition does not influence the overall order of convergence, since we would already expect a convergence order of 1 for shock

waves within one phase. We also check the remeshing routine of the algorithm. We

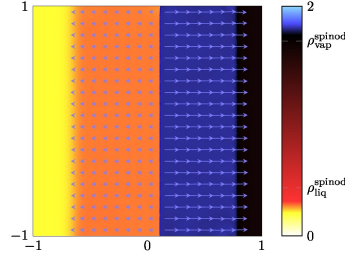


**Fig. 4:** Numerical solution with two shock waves and one phase transition.

$ \mathcal{T}(t) $	$h(\mathcal{T}(t))$	$\ (\mathbf{u}_h - \mathbf{u})(t, \cdot)\ _{L^1}$	EOC(t)
760	$2.0645 \cdot 10^{-1}$	$7.0457 \cdot 10^{-2}$	0.8468
3120	$9.4325 \cdot 10^{-2}$	$3.6295 \cdot 10^{-2}$	1.0986
12757	$5.3309 \cdot 10^{-2}$	$1.9390 \cdot 10^{-2}$	0.7928
50884	$2.6078 \cdot 10^{-2}$	$1.1000 \cdot 10^{-2}$	0.7338
204158	$1.1835 \cdot 10^{-2}$	$6.1603 \cdot 10^{-3}$	

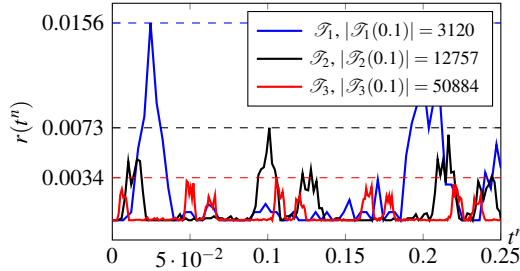
**Table 2:** Experimental orders of convergence (EOC) at time  $t = 0.1$  for the Riemann problem.

compute the relative change in the number of triangles given as

$$r(t^n) = |\hat{I}^{(n)} \setminus I^{(n)}| / |\hat{I}^{(n)}|,$$

where  $I^{(n)}$  is the index set of the mesh  $\mathcal{T}(t^n)$  and  $\hat{I}^{(n)}$  the index set of the mesh  $\hat{\mathcal{T}}(t^n)$  that results from the remeshing of  $\mathcal{T}(t^n)$  such that  $K_i = \hat{K}_i$  is valid for all  $i \in I \cap \hat{I}$ . From Figure 5 it can be seen that the change is decreasing for finer meshes and, for the three moving meshes depicted in the figure, limited by 1.56%, only.

**Fig. 5** Relative change in the number of triangles of the remeshing routine performed after every time step of the algorithm. The three moving meshes correspond to the meshes 2, 3 and 4 of Table 2.



*Example 3 (Oscillating Droplet).* Next, we continue with an example, which involves more intricate geometric dynamics of the interface. This time, the initial condition consists of a liquid droplet surrounded by the fluid in vapour phase.

$$(\rho_0(\mathbf{x}), \rho_0 \mathbf{v}_0(\mathbf{x})) = \begin{cases} (1.7, 0, 0) & \text{if } \|\mathbf{x}\|^2 < 0.2, \\ (0.3, 0, 0) & \text{if } \|\mathbf{x}\|^2 > 0.2 \end{cases}$$

At the boundary we choose reflecting boundary conditions. Figure 6 shows the numerical results, that show how the initial bubble emits a wave to the inside and one wave to the outside of the bubble with a lower jump height (see color scale).

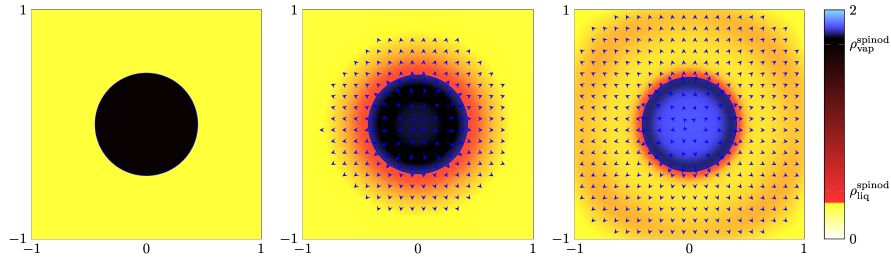


Fig. 6: Numerical solutions for a single droplet surrounded by gas at  $t = 0, 0.5$  and  $1$ .

*Example 4 (Vapour bubbles).* In the next example we will consider a couple of vapour bubbles that start emitting waves and oscillate. The emitted waves interact thereby with the sharp phase boundaries, see Figure 7. For this example we again choose reflecting boundary conditions.

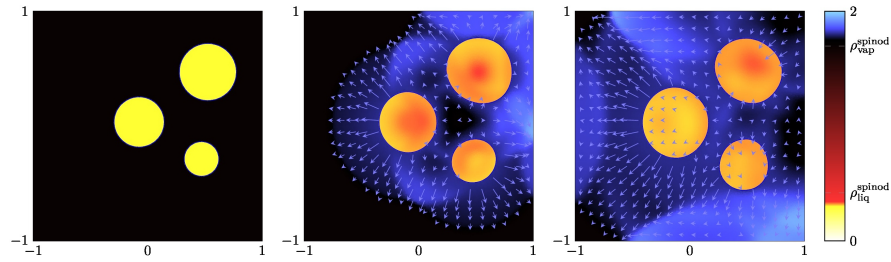


Fig. 7: Numerical solutions for three vapour bubbles in liquid at  $t = 0, 0.5$  and  $1$ .

*Example 5 (With surface tension).* In all previous examples surface tension was neglected. Surface tension can be modeled via a modified Rankine-Hugoniot condition at the phase boundary given as

$$\begin{aligned} \llbracket \rho(\mathbf{v} \cdot \mathbf{n} - \boldsymbol{\sigma}) \rrbracket &= 0, \\ \llbracket \rho(\mathbf{v} \cdot \mathbf{n} - \boldsymbol{\sigma}) \mathbf{v} \cdot \mathbf{n} - p(\rho) \rrbracket &= \zeta^* \kappa \end{aligned}$$

where  $\boldsymbol{\sigma}$  is the velocity of the phase boundary,  $\zeta^* \geq 0$  is a constant surface tension coefficient and  $\kappa = \kappa(\mathbf{x}, t)$  the mean curvature of the interface curve. In this last example we show numerical results where surface tension acts on a deformed droplet. We use again reflecting boundary conditions. Figure 8 shows how the droplet evolves to an equilibrium circular shape.

## References

1. CGAL Computational Geometry Algorithms Library. <http://www.cgal.org>

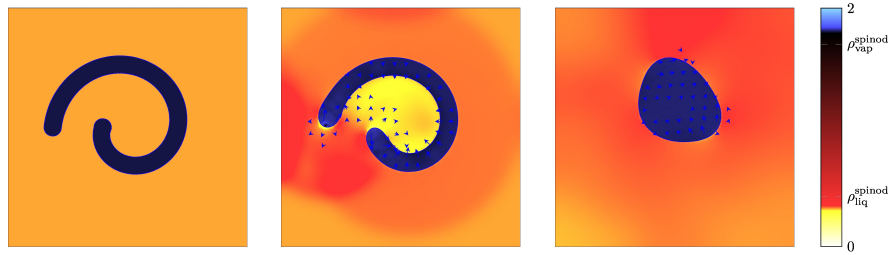


**Fig. 8:** Numerical solutions for a deformed droplet at times  $t = 0, 0.8$  and  $6$ .

2. Abeyaratne, R., Knowles, J.K.: Kinetic relations and the propagation of phase boundaries in solids. *Arch. Rational Mech. Anal.* **114**(2), 119–154 (1991)
3. Berg, M.d., Cheong, O., Kreveld, M.v., Overmars, M.: *Computational Geometry: Algorithms and Applications*, 3rd ed. edn. Springer-Verlag TELOS, Santa Clara, CA, USA (2008)
4. Chalons, C., Coquel, F., Engel, P., Rohde, C.: Fast relaxation solvers for hyperbolic-elliptic phase transition problems. *SIAM J. Sci. Comput.* **34**(3), A1753–A1776 (2012)
5. Chalons, C., Engel, P., Rohde, C.: A conservative and convergent scheme for undercompressive shock waves. *SIAM J. Numer. Anal.* **52**(1), 554–579 (2014)
6. Chalons, C., Rohde, C., Wiebe, M.: A finite volume method for undercompressive shock waves in two space dimensions (2017). DOI <https://doi.org/10.1051/m2an/2017027>
7. Chen, C., Hattori, H.: Exact Riemann solvers for conservation laws with phase change. *Appl. Numer. Math.* **94**, 222–240 (2015)
8. Chertock, A., Karni, S., Kurganov, A.: Interface tracking method for compressible multifluids. *M2AN Math. Model. Numer. Anal.* **42**(6), 991–1019 (2008)
9. Colombo, R.M., Priuli, F.S.: Characterization of Riemann solvers for the two phase  $p$ -system. *Comm. Partial Differential Equations* **28**(7-8), 1371–1389 (2003)
10. Dressel, A., Rohde, C.: A finite-volume approach to liquid-vapour fluids with phase transition. In: *Finite volumes for complex applications V*, pp. 53–68. ISTE, London (2008)
11. Fechter, S., Munz, C.D., Rohde, C., Zeiler, C.: A sharp interface method for compressible liquid-vapor flow with phase transition and surface tension. *J. Comput. Phys.* **336**, 347–374 (2017)
12. Hantke, M., Dreyer, W., Warnecke, G.: Exact solutions to the Riemann problem for compressible isothermal Euler equations for two-phase flows with and without phase transition. *Quart. Appl. Math.* **71**(3), 509–540 (2013)
13. LeFloch, P.G.: *Hyperbolic systems of conservation laws. Lectures in Mathematics ETH Zürich.* Birkhäuser Verlag, Basel (2002)
14. LeFloch, P.G., Thanh, M.D.: Non-classical Riemann solvers and kinetic relations. II. An hyperbolic-elliptic model of phase-transition dynamics. *Proc. Roy. Soc. Edinburgh Sect. A* **132**(1), 181–219 (2002)
15. Merkle, C., Rohde, C.: Computation of dynamical phase transitions in solids. *Appl. Numer. Math.* **56**(10-11), 1450–1463 (2006)
16. Rohde, C., Zeiler, C.: A relaxation Riemann solver for compressible two-phase flow with phase transition and surface tension. *Appl. Numer. Math.* **95**, 267–279 (2015)
17. Truskinovsky, L.: Kinks versus shocks. In: J. Dunn (ed.) *Shock Induced Transitions and Phase Structures in General Media, The IMA Volumes in Mathematics and its Applications*, vol. 52, pp. 185–229. Springer (1993)
18. Zeiler, C.: *Liquid Vapor Phase Transitions: Modeling, Riemann Solvers and Computation.* PhD thesis. Universität Stuttgart (2015)